Achievable Moments NDI-based Fault Tolerant Thrust Vector Control of an Atmospheric Vehicle during Ascent

Andrés Marcos, David Mostaza and Luis F. Peñín

**Deimos Space S.L., Madrid, 28035*
SPAIN (Tel: +34-9180634625; e-mail: andres.marcos, david.mostaza, luis-felipe.penin@ deimos-space.com).

Abstract: In this article the design of a fault tolerant thrust vector control (TVC) for the automated ascent of the Hopper reusable launch vehicle is presented. The considered ascent starts at the pull-up maneuver performed immediately after horizontal take off and ends at main-engine-cut-off. The TVC law uses nonlinear dynamic inversion (NDI) to obtain the required engine gimbal deflections for robust tracking of the angle of attack and bank angle from a guidance law. The NDI–based TVC is characterized by the use of the Hopper's engine redundancy layout and by the interpretation of NDI as an achievable dynamics identification scheme. The resulting TVC design has been validated using a Monte Carlo campaign with realistic aerodynamic mismatch, corrupted measurements, parametric uncertainty and high fidelity atmospheric and 6DoF vehicle dynamics models. Evaluation of the design with a wide array of thrust and engine gimbal faults yields that the resulting TVC improves the closed loop fault tolerant capabilities.

1. INTRODUCTION

In this article the design of a nonlinear dynamic inversion thrust vector control system for the ascent phase of the Hopper Reusable Launch vehicle (RLV) is described. The ascent phase considered starts at the pull-up manoeuvre performed immediately after horizontal take off and ends at main-engine-cut-off (MECO). The design is part of the European Space Agency (ESA) "Health Management Systems for Reusable Launch Vehicles" project lead by EADS-Astrium (Germany) with the objective of assessing, developing and testing HMS and fault detection and isolation (FDI) algorithms for all the RLV main components (G&C, engines and structural airframe).

The selection of NDI [3, 4, 9] as the control design technology for the TVC is motivated by the hardware redundancy offered by the Hopper's three Vulcain engines layout and the possibility of interpreting NDI as an achievable dynamics identification scheme [8]. The resulting ascent NDI TVC design is validated using the high-fidelity closed-loop Hopper FES in a Monte Carlo campaign using parametric and aerodynamic coefficients uncertainties. The results indicate that the TVC helps the ascent G&C design to robustly achieve the desired design objectives while improving the fault tolerance of the closed-loop in the presence of a significant array of faults.

2. REFERENCE SCENARIO

The selected reference vehicle and scenario is that of the Hopper, which is an evolution from the FESTIP study further elaborated in the scope of the ASTRA program [10]. The Hopper mission is to execute sub-orbital point-to-point flights for delivery of orbital payloads. The mission sequence is: accelerate to prescribed sub-orbital staging conditions, ejection of payload, drift to ~150 km altitude, automated atmospheric re-entry and glide to the selected landing site (some 4500 km downrange depending on mission inclination). The duration of a Hopper flight is less than half an hour from horizontal take-off until the vehicle arrives over the downrange landing site. The phase of interest for the HMS ascent TVC design starts from the moment the Hopper has initiated the pull-up manoeuvre after the horizontal sled-driven take off and ends at MECO, around 96 Km of altitude and Mach 18. Fig. 1 shows the main rotational and aerodynamic profiles for the reference ascent trajectory.

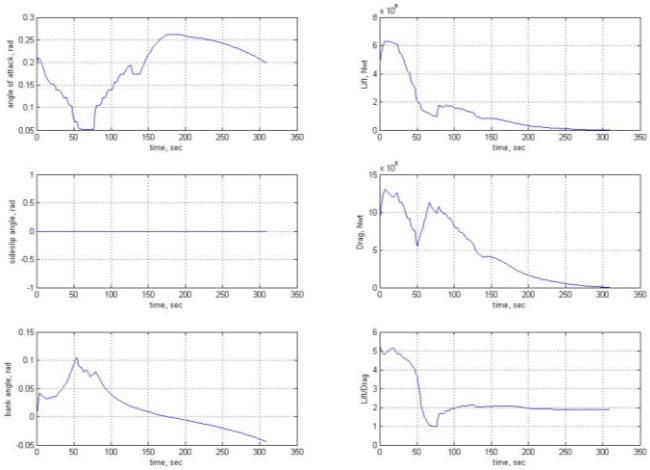

Fig. 1 Hopper's ascent reference trajectory: rotational and aerodynamics parameters

The general G&C design objectives consist in robust and accurate tracking of the reference guidance (γ_{ref}, χ_{ref}) and calculated aerodynamic (α_{calc}, β_{calc}, σ_{calc}) angles, reduced control activity and stability throughout the flight despite the presence of parametric uncertainty, sensor noise and aerodynamic mismatch, see [6] for more details.

The main challenges for the Hopper ascent guidance and control (G&C) design are the result of the large dynamical

changes (e.g. from Mach 0 to 18), the large mass variation occurring from the engine fuel consumption (a change from 491,288 kg down to 90,000 kg) and the mass variation effect on the moments of inertia and center-of-gravity. Additionally, system uncertainty from parametric (moment of inertia, mass, center-of-gravity position) and aerodynamic mismatch is also considered using a multiplicative formulation [1] that allows defining the uncertainty in terms of percentage variations with respect to nominal values. The aerodynamic mismatch is introduced to recreate the uncertainty that exists in the calculation of aerodynamic databases, which are intrinsically very difficult to identify, and to avoid perfect cancellation of the dynamics due to the inversion performed in NDI controllers. Fig. 2 shows the Mach-based aerodynamic coefficients' uncertainty profiles used to perturb the Hopper aerodynamic database. These profiles are used to scale the aerodynamic coefficients during a Monte Carlo assessment campaign, and it is highlighted that the profiles for the lift and drag uncertainties are correlated by a lift-to-drag uncertainty profile in order to be physically motivated.

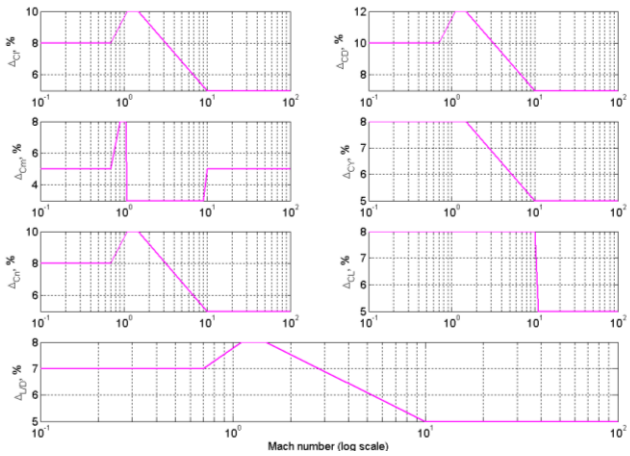

Fig. 2 Aerodynamic coefficients uncertainty profiles

An additional challenge (especially in comparison to that for unpowered re-entry) arises from the engine thrust and gimballing capabilities, which favours the use of a TVC unit within the attitude control component of the ascent G&C.

The Hopper RLV has three Snecma Vulcain main engines that can be gimballed independently (i.e. each with its own actuator system) in pitch and yaw directions, see Fig. 3:

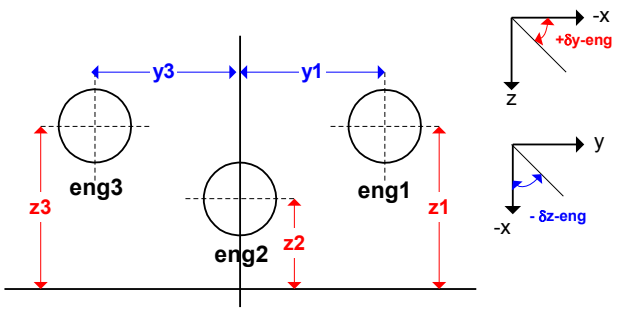

Fig. 3 Hopper engines position (from rear view) and deflection angle sign convention

For each engine, the actual engine forces are calculated based on the provided engine thrust *Tn* and the commanded engine gimbal deflections for that engine, δy_{eng} for pitch and δz_{eng} for yaw. In body frame, the engine forces are expressed as in Eq. 1 (to calculate the total body-axes forces, the engine forces are first transformed to wind-axes prior to being added to the aerodynamic forces):

$$F_{eng} = \begin{bmatrix} F_{Xeng} \\ F_{Yeng} \\ F_{Zeng} \end{bmatrix} = \begin{bmatrix} Tn \cos\delta y_{eng} \cos\delta z_{eng} \\ Tn \cos\delta y_{eng} \sin\delta z_{eng} \\ -Tn \sin\delta y_{eng} \end{bmatrix} \qquad \text{Eq.1}$$

The engine moments are calculated using the body-axes engine forces and the distance measured from the engine nozzle reference point to the center of gravity as the moment-arm to yield, $r = nozzle - r_{cg} = [x_{eng}\ y_{eng}\ z_{eng}]$:

$$M = \begin{bmatrix} 0 & -z_{eng} & y_{eng} \\ z_{eng} & 0 & -x_{eng} \\ -y_{eng} & x_{eng} & 0 \end{bmatrix} \begin{bmatrix} F_{Xeng} \\ F_{Yeng} \\ F_{Zeng} \end{bmatrix} \qquad \text{Eq. 2}$$

It is noted that the matrix in the right term of Eq. 2 has no inverse (an important consideration if NDI techniques are directly used for thrust vector control).

3. ASCENT NDI CONTROL LAW DESIGN

In [7] a G&C design for the Hopper vehicle during ascent was presented. The design includes an attitude control law that contains four major components, from left to right: a PID-plus-Rotational-Equations-Of-Motion-Inversion block that estimates desired moments based on the guidance law calculated aerodynamic angles; a Moment-Allocation block, in charge of distributing these estimated ideal moments to the appropriate effectors (aerodynamic surfaces, thrust vector control and reaction control system); an Aerodynamic-Moment-Inversion component that transforms the ideal aerodynamic moments into commanded aerodynamic control surface deflections; and the TVC component, which uses the allocated engine ideal moments (and available engine thrusts) to calculate the required engine gimbals' deflections per engine. Each of the first three elements is described in detail in [7] and the TVC is described next.

3.1 Thrust Vector Control Design

The TVC component represents a major innovative component of the Hopper vehicle for G&C development since the redundancy offered by the three engines allow to obtain closed-loop fault tolerance capabilities against engine faults –due to the three engine architecture—and against aerodynamic actuator faults –by providing an additional moment effector capability.

The TVC block main mission is to calculate the engines' gimbal deflections required to achieve the allocated engine moments (that is, it does not provide thrust modulation control). The approach and implementation used is developed with the goal to simplify the design and tuning of the TVC but also looking for a mean to naturally provide some

inherent fault accommodation capability by taking advantage of the offered engine hardware redundancy.

Before describing the TVC implementation, first combine the equations for the body-axes engine forces from Eq. 1 and that for the moments Eq. 2 to get the individual engine moments in terms of thrust and gimbal deflections. Assuming that the trigonometric expressions can be approximated using small angle (based on the maximum gimbals deflection of ±14 degrees), Eq. 3 is obtained:

$$\begin{bmatrix} M_{Xeng} \\ M_{Yeng} \\ M_{Zeng} \end{bmatrix}_{eng-i} \approx \begin{bmatrix} -Tn(y_{eng}\delta y_{eng} + z_{eng}\delta z_{eng}) \\ Tn(z_{eng} + x_{eng}\delta y_{eng}) \\ Tn(x_{eng}\delta z_{eng} - y_{eng}) \end{bmatrix}_{eng-i} \qquad \text{Eq. 3}$$

Next, summing the contribution from each engine and re-arranging in the unknown gimbal deflections, the total engine moments are obtained:

$$\begin{bmatrix} M_{Xeng} \\ M_{Yeng} \\ M_{Zeng} \end{bmatrix} = \sum_{i=1}^{3} \begin{bmatrix} -Tn \cdot y_{eng} & -Tn \cdot z_{eng} \\ Tn \cdot x_{eng} & 0 \\ 0 & Tn \cdot x_{eng} \end{bmatrix}_i \begin{bmatrix} \delta y_{eng} \\ \delta z_{eng} \end{bmatrix}_i + \begin{bmatrix} 0 \\ \sum_{i=1}^{3} Tn_i \cdot z_{eng-i} \\ -\sum_{i=1}^{3} Tn_i \cdot y_{eng-i} \end{bmatrix} \qquad \text{Eq. 4}$$

Eq. 4 can be simplified using the engines position symmetry, see Fig. 3: $x_{eng1} = x_{eng2} = x_{eng3}$, $y_{eng1} = -y_{eng3}$, $z_{eng1} = z_{eng3}$ and $y_{eng2} = 0$.

$$\begin{bmatrix} M_{Xeng} \\ M_{Yeng} \\ M_{Zeng} \end{bmatrix} = -B + A\Gamma = -\begin{bmatrix} 0 \\ z_{eng1}(Tn_1 + Tn_3) + z_{eng2}Tn_2 \\ y_{eng1}(Tn_3 - Tn_1) \end{bmatrix} +$$

$$\begin{bmatrix} -Tn_1 y_{eng1} & -Tn_1 z_{eng1} & 0 & -Tn_2 z_{eng1} & -Tn_3 y_{eng1} & -Tn_3 z_{eng1} \\ Tn_1 x_{eng1} & 0 & Tn_2 x_{eng1} & 0 & Tn_3 x_{eng1} & 0 \\ 0 & Tn_1 x_{eng1} & 0 & Tn_2 x_{eng1} & 0 & Tn_3 x_{eng1} \end{bmatrix} \begin{bmatrix} \delta y_{eng1} \\ \delta z_{eng1} \\ \delta y_{eng2} \\ \delta z_{eng2} \\ \delta y_{eng3} \\ \delta z_{eng3} \end{bmatrix} \qquad \text{Eq. 5}$$

Typically, the standard NDI approach proceeds by calculating matrices A and B in the above equation, subtracting the latter from the total allocated engine moments and left-multiplying the result by the inverse of A to get the desired gimbal deflection vector Γ as shown in Eq. 6:

$$\Gamma = \boldsymbol{W} \cdot [\boldsymbol{AW}]^{+} (\boldsymbol{M} + \boldsymbol{B}) \qquad \text{Eq. 6}$$

Where $[\cdot]^{+}$ indicates Moore-Penrose pseudo inverse and W is a regularization matrix used to avoid ill conditioning (but that can be used as well as a tuning parameter to adequately weight the problem or for allocation issues [2, 3]).

This standard approach was attempted first and good results were obtained for the initial phase of the ascent but with incremental tuning difficulty when PID-gains and moment allocation switching phases were considered. Furthermore, although the nature of the NDI approach provides some level of fault accommodation it is not straightforward to include reconfiguration-tuning provisions. Additionally, and more importantly, it was noted before that the matrix A in Eq. 5 has no inverse and thus numerical issues regarding regularization (i.e. use of appropriate W) must be carefully considered to avoid singularities, thus resulting in a more complex design and validation process.

Based on the above remarks, a different NDI-TVC approach is proposed that facilitates comprehension and tuning of the resulting system. The approach is based on performing an additional TVC-internal engine moment allocation phase followed by a sequential inversion scheme that calculates the engine gimbal deflections using an achievable moment estimation mid-step:

Step 1: Distribute the allocated engine moments from the main Moment-Allocation block among the side engines (that for the central engine, number 2 in Fig. 3, is calculated in Step3). This allocation is currently performed by simply assigning a percentage of the total engine moment to each of the engines. Information from HMS and/or engine-FDI can be used to change the assigned moments providing a direct channel to influence the engine gimbal calculation.

Step 2: Use dynamic inversion to calculate individually the side engines' gimbal. It is noted that the inversion is very straightforward due to the symmetric engine layout. Indeed, no regularization or other mathematical numerical tool is required as seen in Eq. 7 (each moment, thrust and position coordinate in the equation must be assumed to be specific to the side engine considered, *i=1, 3*).

$$\delta y_{eng-i} = \frac{M_{Yeng-i} - z_{eng-i} Tn_{eng-i}}{x_{eng-i} Tn_{eng-i}}$$
$$\delta z_{eng-i} = \frac{M_{Zeng-i} + y_{eng-i} Tn_{eng-i}}{x_{eng-i} Tn_{eng-i}} \qquad \text{Eq. 7}$$

Note that for zero moment case non-zero deflections are obtained, $\delta y_{eng} = -z_{eng}/x_{eng}$ and $\delta z_{eng} = y_{eng}/x_{eng}$. Indeed, due to the y-axis symmetry of the side engines ($y_{eng1} = -y_{eng3}$) their contribution to the total z-axis engine moment Mz_{eng} cancels out if there are no faults and the engines' thrusts are equal. Thus, unless the individual side z-axis moments Mz_{eng-i} are somehow corrected, this symmetry can potentially result in non-zero and opposite gimbal deflections for zero moment. In order to avoid this situation, each allocated side engine z-axis moment $M_{allocated-zeng-i}$ is corrected to result in zero deflection for zero moment prior to be used in Eq. 7:

$$M_{zeng-i} = M_{allocated-zeng-i} - y_{eng-i} Tn_{eng-i} \qquad \text{Eq. 9}$$

Step 3: This step provides a measure of the moments achieved by the side engines and uses these estimates together the total engine allocated moment to calculate the required moment for engine 2. Similar to the first step, any fault information available can be used here in a very simple manner. For example, if a side gimbal fault is identified by the HMS or engine-FDI, the calculated 'fault-free' gimbal deflection in the previous step can be modified in order to estimate the moment that the side engine will achieve. Note that for the fault-free case, the estimated side engines' moments should be very similar to the achieved one and thus the central engine moments will be equal to the total allocated engine moments minus the side engines' moments assigned in Step 1. In contrast, for the faulty case, this step

will estimate the deviation from the demanded side engines' moments and compensate accordingly the allocated central engine moments:

$$\begin{aligned}\tilde{M}_{Xeng2} &= M_{Xeng} - \sum_{1,3}\tilde{M}_{Xeng} = M_{Xeng} + \sum_{1,3} Tn_{eng}(y_{eng}\delta y_{eng} + z_{eng}\delta z_{eng}) \\ \tilde{M}_{Yeng2} &= M_{Yeng} - \sum_{1,3}\tilde{M}_{Yeng} = M_{Yeng} - Tn_{eng}(x_{eng}\delta y_{eng} + z_{eng}) \\ \tilde{M}_{Zeng2} &= M_{Zeng} - \sum_{1,3}\tilde{M}_{Zeng} = M_{Zeng} - Tn_{eng}(x_{eng}\delta z_{eng} - y_{eng})\end{aligned} \quad \text{Eq. 9}$$

Step 4: This final step calculates the engine 2 gimbal deflections using the allocated moment from the previous step in a similar manner to Step 2. Note in Eq. 10 that the yaw central engine deflection $\delta z_{eng\text{-}2}$ only uses the z-axis moment as the result of the engine being collocated with the x body-axis. Nevertheless, it is observed from Eq. 9 that $M_{Xeng\text{-}2}$ could have been used instead of $M_{Zeng\text{-}2}$, or alternatively a linear combination of both, but the inversion from Eq. 10 gave better results and facilitated canceling sideslip accelerations:

$$\delta y_{eng-2} = \frac{M_{Yeng-2} - z_{eng-2}Tn_{eng-2}}{x_{eng-2}Tn_{eng-2}}$$

$$\delta z_{eng-2} = \frac{M_{Zeng-2}}{x_{eng-2}Tn_{eng-2}} \quad \text{Eq. 10}$$

4. CLOSED LOOP NO-FAULT MONTE CARLO

In this section the performance and robustness of the complete NDI G&C design in tracking the reference ascent nominal trajectory is evaluated (an earlier NDI G&C design was used in [7], but there the TVC used provided non-zero deflections for non-zero moments).

A Monte-Carlo (MC) analysis using random perturbation of the uncertainty set formed by the parametric and aerodynamic database uncertainty given before is performed for 1000 runs. The simulation environment used has the following features:

- Full 6 Degree-of-Freedom nonlinear RLV dynamics
- High-fidelity Hopper aerodynamic database
- 1962 USA atmospheric and ellipsoid planet shape
- Actuators are always magnitude and rate limited. The aerodynamic and engine gimbal actuators include also 2nd order actuator dynamics
- Sensor measurements are corrupted by colored noise (except for the accelerometers, which use white noise)

Additionally, it is assumed that the given reference total thrust profile is equally split for each of the three Hopper engines. Tests with the high-fidelity Snecma engine models were also performed for a selected set of uncertainty scenarios and yielded satisfactory results (the engine model time constant does not allow for efficient MC campaign).

Fig. 4 and Fig. 5 present the time responses of the measured guidance angles (γ, χ) and aerodynamic angles (α, β, σ) respectively, together their errors with respect to the corresponding reference signals (γ_{ref}, χ_{ref}, α_{calc}, β_{calc}, σ_{calc}) for a set of the 1000 MC runs performed (the results are representative of the 1000 cases). Note, that the guidance reference angles are those from the optimized ascent trajectory while the aerodynamic angles are obtained from the guidance law (and thus are not fixed profiles as γ_{ref} and χ_{ref}). This implies that the plots in the left of Fig. 5, corresponding to the aerodynamic angles time responses, show a larger spread than those for the guidance angles in Fig. 4 (although the errors shown in the right-side plots indicate that the NDI G&C performs very well for all).

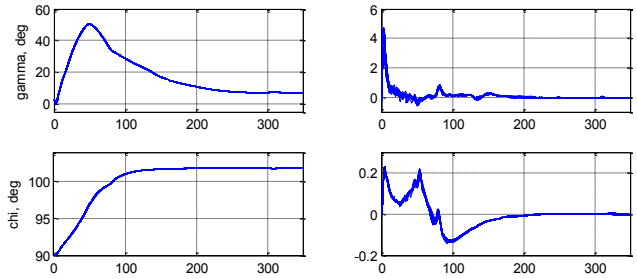

Fig. 4 Monte Carlo (100-of-1000 runs): guidance angles

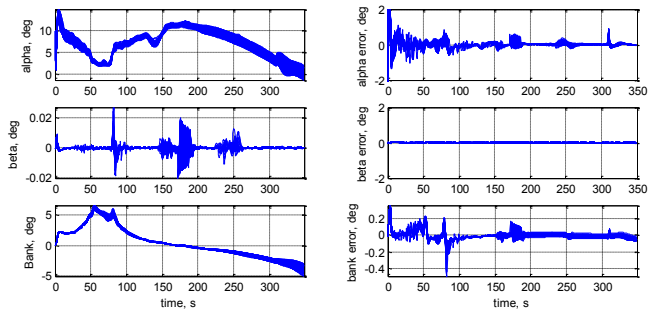

Fig. 5 Monte Carlo (100-of-1000 runs): control angles

Fig. 6 shows the TVC gimbal deflections and the thrust provided by each engine. Since the latter engine thrusts are obtained by dividing the total thrust profile given in the reference trajectory in equal parts, the resulting responses shown at the bottom plot coincide. The abrupt reduction in thrust seen around 308 seconds is the result of a 10% reduction in thrust commanded in preparation for MECO.

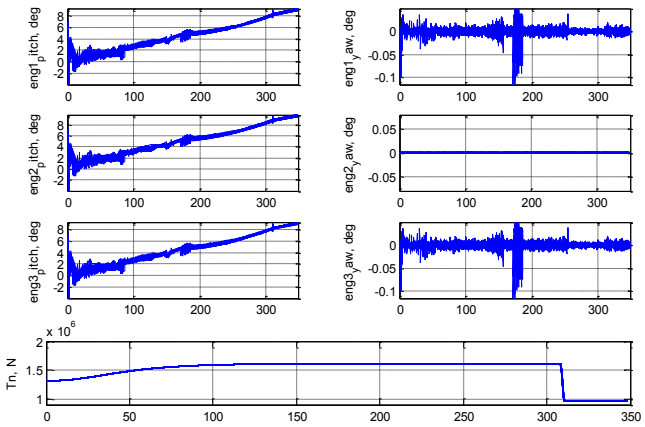

Fig. 6 Monte Carlo (100-of-1000): TVC deflections & thrust

With respect to the observed pitch (left) and yaw (right) engine gimbal deflections in Fig. 6, first recall that the G&C design is developed so that the aerodynamic surface activity

is smoothly reduced at high speeds (from approximately a flight time of 225 seconds onwards) to avoid damage. Additionally, at this high altitude region the associated reduction in dynamic pressure results in a loss of aerodynamic surface effectiveness. These two considerations imply that final RLV steering must be performed using the engine gimbal deflections (and of course, RCS). This is especially the case for longitudinal control and is easily appreciated in the left column of Fig. 6 that shows the pitch engine deflections progressively increasing. Since all engines have the same x-axis nozzle coordinate and the same thrust is assumed, the engines pitch deflections are almost the same. For the yaw gimbal deflections, shown in the right-side plots of Fig. 6, it is seen that they are mostly zero (since the Monte Carlo campaign assumed no-faults, the central engine yaw deflection is exactly zero). This is a reflection of the almost zero sideslip desired trajectory.

5. CLOSED LOOP FAULT EVALUATION

In this section, a time-domain evaluation of the closed loop fault tolerance to TVC faults is performed. A wide array of fault types (bias, drift LOF, LIP and dead) with different magnitudes are tested for the thrust and gimbals in engine 1 and for the thrust of engine 2. In the current evaluation, no FDI information is used within the moment allocation or the estimated achievable moment TVC steps.

The first fault shown corresponds to an engine 1 yaw gimbal fault with a 10 percent positive bias occurring after 25 seconds of starting the ascent. Fig. 7 shows the control angles, blue-solid for the 'fault' case and red-dashed for the 'no-fault'. It is easily observed the strong change in the guidance-calculated inner-loop angles, which does not have any consequence since the error in the tracking of the 'fault' control angles is still within limits. It is also noted that the change between the guidance angles for the 'fault' and 'no-fault' case was quickly accommodated indicating that the closed-loop can sustain strong biases in the yaw gimbals for the side engines (since they are symmetric, results for one of them mirrors those for the other).

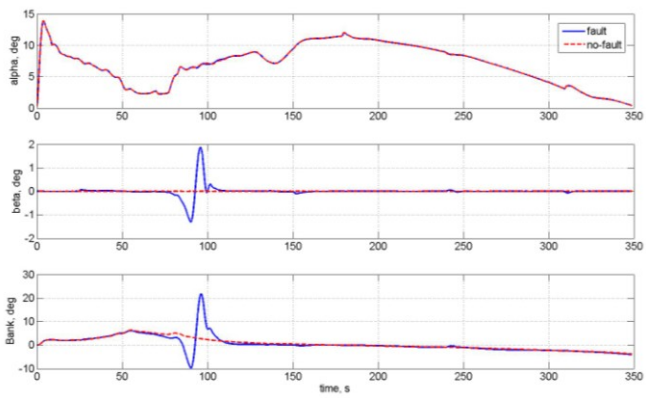

Fig. 7 Fault [$\delta z_{eng\text{-}1}$, +10% bias, at 25 sec]: control angles

Fig. 8 and Fig. 9 show respectively the corresponding aerodynamic and TVC deflections. Note the slight difference in the aerodynamic deflections seen in Fig. 8. On the other hand, Fig. 9 shows a positive deflection of $\delta z_{eng\text{-}1}$ as a result of the introduced fault, and an almost similar but opposite deflection for $\delta z_{eng\text{-}3}$ that compensates the effects of the fault (i.e. except for the abrupt change around 80-100 seconds, no noticeable difference in the control angles occurs as it was seen in Fig.7). Indeed, it is noted that similar results were obtained for all types of faults (except dead) in $\delta z_{eng\text{-}1}$.

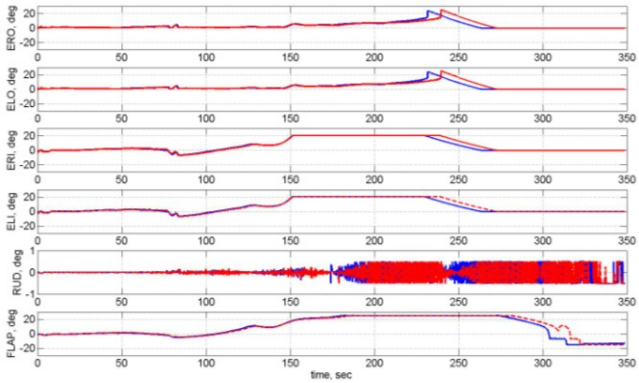

Fig. 8 Fault [$\delta z_{eng\text{-}1}$, +10% bias, at 25 sec]: aero deflections

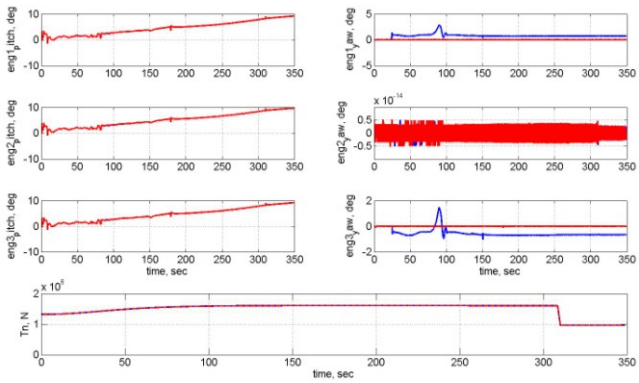

Fig. 9 Fault [$\delta z_{eng\text{-}1}$, +10% bias, at 25 sec]: TVC deflections

Evaluating the same type of fault (a positive 10% bias at 25 seconds after start) but for the thrust provided by engine 1 and engine 2 provides more insight into the FTC behaviour of the TVC. Fig. 10 compares the yaw gimbal deflections for the engine 1 thrust fault (3 left-top plots) and those for the engine 2 thrust fault (3 right-top plots). The bottom plot of the figure shows the positive 10% bias used in the thrust (same profile for both fault cases). Observe the radically different behaviour for the two fault cases. For the *Tn1* fault (left), the required side engine 1 deflection for the same moment is smaller due to the stronger (i.e. biased) force used. This effect is reduplicated by the side engine 3 and the net fault moment effect cancelled out by deflecting the central engine in opposite direction. For the *Tn2* fault (right), since the engine affected is the central, there is not really a noticeable effect at the TVC level since the calculated engine 2 yaw-moment is zero if there are no faults in the other engines' yaw gimbals.

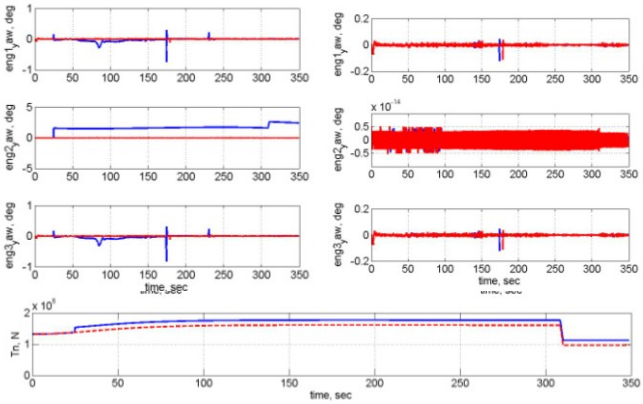

Fig. 1 Faults [Tn1 (left) / Tn2 (right), +10% bias, at 25 sec]: TVC deflections and thrust (bottom)

6. CONCLUSIONS

A thrust vector controller has been design for the ascent phase of the Hopper RLV. The design has used NDI to exploit the vehicle's engine redundancy and take advantage of the possibility to interpret NDI as an achievable dynamic scheme. The resulting TVC design imbues the closed loop with fault tolerance properties in a very natural manner. A nonlinear high-fidelity functional engineering simulator has been used to validate the complete ascent G&C design with very good results. A fault evaluation with the same nonlinear simulation has been performed and the results indicate that the NDI-TVC approach provides closed loop fault tolerance to engine faults.

ACKNWOLEDGEMENT

The authors gladly thank and acknowledge the help of Josef Sommer and Wolfgang Belau from EADS-Astrium Space Transportation (Germany) and Eric Bornschlegl from ESA ESTEC.

REFERENCES

[1] Balas, G.J., Doyle, J.C., Glover, K., Packard, A., Smith, R., (2001) *mu-Analysis and Synthesis Toolbox*, The Mathworks & MUSYN Inc.

[2] Enns, D., (1998) Control Allocation Approaches, *AIAA Guidance, Navigation and Control Conference*, Boston

[3] Honeywell and Lockheed Martin (1996) *Application of Multivariable Control Theory to Aircraft Control Laws*, Technical Report WL-TR-96-3099

[4] Ito, J. Georgie, J. Valasek and D.T. Ward (2001), *Re-entry Vehicle Flight Controls Design Guidelines: Dynamic Inversion*, Final Technical Report NAG9-1085

[5] Kerr, M., Marcos, A., Peñín, (2009) Development of an FDI Filter for the Hopper RLV during Re-entry, *IFAC Safeprocess 2009,* Barcelona, submitted

[6] Marcos, A., Peñín, L.F., Caramagno, A., Sommer, J., Belau, W., (2007) Atmospheric Re-Entry NDI Control Design for the Hopper RLV Concept, *17th IFAC Symposium on Automatic Control in Aerospace*, Toulouse

[7] Marcos, A., Peñín, L.F., (2008) Guidance and Control Design for the Ascent phase of the Hopper RLV, *AIAA Guidance, Navigation and Control Conference*, Hawaii

[8] Ostroff, A.J., Bacon, B.J., (1999) Force and Moment Approach for Achievable Dynamics using Nonlinear Dynamic Inversion. *AIAA Guidance, Navigation and Control Conference,* Portland

[9] Snell, S.A., (1991) *Nonlinear Dynamic-Inversion Flight Control of Supermaneuverable Aircraft*. PhD. Thesis, Dept. Aerospace and Eng. Mechanics, University of Minnesota.

[10] Spies, J. (2002) RLV Hopper: Consolidated System Concept, *53rd International Astronautical Congress*, Texas